

Radiomic features of multi-parametric MRI present stable associations with analogous histological features in brain cancer patients

Samuel Bobholz^a, Allison Lowman^b, Alexander Barrington^c, Michael Brehler^b, Sean McGarry^a, Elizabeth J. Cochran^d, Jennifer Connelly^e, Wade M. Mueller^f, Mohit Agarwal^b, Darren O'Neill^b, Anjishnu Banerjee^g, Peter S. LaViolette^{b,c}

^a*Department of Biophysics, Medical College of Wisconsin*

^b*Department of Radiology, Medical College of Wisconsin*

^c*Department of Biomedical Engineering, Medical College of Wisconsin*

^d*Department of Pathology, Medical College of Wisconsin*

^e*Department of Neurology, Medical College of Wisconsin*

^f*Department of Neurosurgery, Medical College of Wisconsin*

^g*Department of Biostatistics, Medical College of Wisconsin*

Abstract

MR-derived radiomic features have demonstrated substantial predictive utility in modeling different prognostic factors of glioblastomas and other brain cancers. However, the biological relationship underpinning these predictive models has been largely unstudied, with the generalizability of these models also called into question. Here, we examine the localized relationship between MR-derived radiomic features and histology-derived histomic features using a dataset of 16 brain cancer patients. Tile-based radiomics features were collected on T1W, post-contrast T1W, FLAIR, and DWI-derived ADC images acquired prior to patient death, with analogous histomic features collected for autopsy samples co-registered to the MRI. Features were collected for each original image, as well as a 3D wavelet decomposition of each image, resulting in 837 features per MR image and histology image. Correlative analyses were used to assess the degree of association between radiomic-histomic pairs for each MRI. The influence of several confounds were also assessed using linear mixed effect models for the normalized radiomic-histomic distance, testing for main effects of scanners from different vendors and acquisition field strength. Results as a whole were largely heterogenous, but several features demonstrated substantial associations with their histomic analogs, particularly those derived from the FLAIR and post-contrast T1W images. These most-associated features typically presented as stable across confounding factors as well. These data suggest that a subset of radiomic features are able to consistently capture texture information about the underlying tissue histology.

Keywords: Radiomics, MRI, Glioma, Brain Cancer

1. Introduction

Gliomas are an aggressive and often deadly form of primary intracranial tumor, representing 81 percent of malignant brain tumors (1). Current standard treatment includes sur-

gical removal of the tumor followed by administration of radiation and chemotherapy (2,3). Critical to maximizing the efficacy of these treatments is the detection of interval tumor progression and monitoring areas of potential treatment effect using non-invasive imaging. Multiparametric magnetic resonance imaging (MP-MRI) is central to diagnosing a glioma, monitoring its progression, and assessing the efficacy of treatment, as well as providing information regarding neuroanatomy and the physical properties of the tissues. Typical clinical protocols include pre and post-contrast T1-weighted images (T1, T1+C), and T2-weighted fluid attenuation inversion recovery (FLAIR) images, attempting to delineate enhancing, non-enhancing, and necrotic tumor components (4,5). Diffusion-weighted images are also often collected in order to calculate the apparent diffusion coefficient (ADC) map, which is used prognostically to identify areas of restricted diffusion that may manifest as tumor recurrence (68) or stroke (911). Despite their current utility, advancements in clinical imaging and tumor monitoring are necessary to more accurately identify the active, non-enhancing tumor components and inform improved treatment directions.

Recently, MP-MRI has been used for a quantitative feature extraction process known as radiomics. These radiomic features attempt to quantify aspects of an image such as intensity distributions, spatial relationships, and textural heterogeneity (1215). Feature extraction is typically calculated over a given region of interest (ROI), with shape-based features, histogram-based first order features, and a range of texture features across transformations of the original ROI matrix (16). Extensions of these pipelines have also calculated similar features for 3-D wavelet decompositions of the original image, which decompose the original image into its high and low frequency components and provide enriched edge-related information (17,18). The end result of these image processing techniques are mineable datasets of quantitative information that can be compared to clinically relevant metrics. In studies of Glioblastoma Multiforme (GBM) and other brain cancers, several groups have demonstrated the utility of radiomic features in predicting prognostic factors such as survival time, anti-angiogenic treatment response, IDH1 mutation status, and differentiation of GBM from central nervous system lymphomas as well as lower grade astrocytomas (1923).

Despite the promising results shown with standard radiomics-based techniques, several methodological limitations have prevented their widespread adoption. Questions regarding the generalizability of radiomics-based predictive models have been raised by studies assessing the stability of the features across MR acquisition parameters (2427). Current studies of radiomic features tend to focus on feature extractions across the whole tumor for subject-level classification, but studies of localized radiomic features have been limited. Both the clinical need for better localization of active, non-enhancing tumor and the desire for biological validation of radiomics-based signatures further highlight this gap in the current literature. An initial step in bridging this gap is to demonstrate localized associations between radiomic features and similar features of the underlying histology in order to demonstrate congruence between MR-derived features and features of the underlying tissue.

In order to address this initial step towards localized radiomics-based modeling, this study compares localized radiomic features to similarly calculated features of co-registered histology images, referred to here as histomic features. This study uses MRI co-registered tissue samples from brain cancer patients acquired at autopsy to explore the association between tile-based radiomic features and their histomic analogs. Specifically, this study tests the hypotheses that 1) radiomic features demonstrate substantial associative relationships

with their historic analogs, 2) the relationship between radiomic and historic features is stable across scanner vendors and acquisition field strengths.

2. Methods

SUBJECT	AGE (YEARS)	SEX	OVERALL SURVIVAL (MONTHS)	INITIAL DIAGNOSIS	FINAL DIAGNOSIS	TREATMENTS	TIME FROM SCAN TO DEATH (DAYS)	SCANNER VENDOR	FIELD STRENGTH (TESLA)
1	71	M	12	G4 astrocytoma	GBM	Bev, Lom, Rad, Tem	12	GE	3
2	34	M	135	brainstem glioma	G3 Anaplastic astrocytoma	Bev, Vin, Thio, Carbo, Interf	95	Siemens	1.5
3	59	M	17	GBM	GBM	Bev, PLDR, Iso, 2nd surgery, Duke ERADICATE study	42	GE	1.5
4	58	M	26	GBM	GBM	Bev, PLDR, Lom, BCNU, Tem	114	Siemens	1.5
5	64	M	19	GBM	GBM	Bev, PLDR, Chemo	37	GE	3
6	62	F	8	GBM	GBM	Bev, Tem, repeat surgery	13	GE	3
7	88	M	4*	GBM	GBM	Bev, TTF, Irin, Rad, Tem	47	GE	1.5
8	78	F	147	GBM	GBM	TTF, Chemo	90	GE	3
9	75	F	10	GBM	GBM	Bev, Rad, Tem, Lom, TTF	22	GE	1.5
10	55	M	17	GBM	GBM	TTF, Rad, Dec, PPI	16	GE	3
11	56	M	30	G3 anaplastic oligo	G3 anaplastic oligo	Chemo, Rad	75	GE	1.5
12	41	M	11	GBM	GBM	Rad, Chemo, TTF	22	GE	1.5
13	62	F	10	GBM	GBM	TTF, Rad, Chemo, Eno	7	GE	3
14	54	M	12	GBM	GBM	Bev, Rad, Tem, PLDR	27	GE	3
15	85	M	13	GBM	Extensive treatment effect	Rad, Chemo	65	GE	3
16	68	F	24	GBM	GBM	Optune	184	GE	3

Table 1: Demographic and Clinical Characteristics of Sample. Overall survival time is calculated from first surgery, except in case denoted with *, in which case surgery was not performed and survival is calculated from first appearance on MRI. Bev = bevacizumab, Lom = Lomustine, Tem = Temozolomide, Vin = Vincristine, Thio = Thio triethylene thiophosphoramidate, Carb = carbamazepine, RNAI = RNA interference therapy, PLDR = pulsed low-dose rate radiotherapy, Iso = isotretinoin, Irin = irinotecan, Car = carmustine, Chemo = unspecified chemotherapy, Rad = unspecified radiation therapy, TTF = tumor treating fields, Dec = dexamethasone, PP1 = polyphyllin I, Eno = enoxaparin sodium.

2.1. Patient Population

Sixteen patients with pathologically confirmed primary brain tumors were enrolled for the brain tissue component of this IRB approved study. A brief outline of the clinical history of each subject is presented in Table 1 and a diagrammatic representation of the data collection process is presented in Figure 1.

2.2. Image Acquisition and Preprocessing

T1-weighted pre- and postcontrast images (T1 and T1+C, respectively), diffusion weighted images, and Fluid-attenuated inversion recovery (FLAIR) images were acquired from each subject prior to death for clinical purposes. Images were acquired on our institutional MRI scanners, including 1.5T and 3T GE (General Electric Health, Waukesha, Wisconsin) and Siemens (Siemens Healthineers, Erlangen, Germany) magnets. Acquisition parameters for

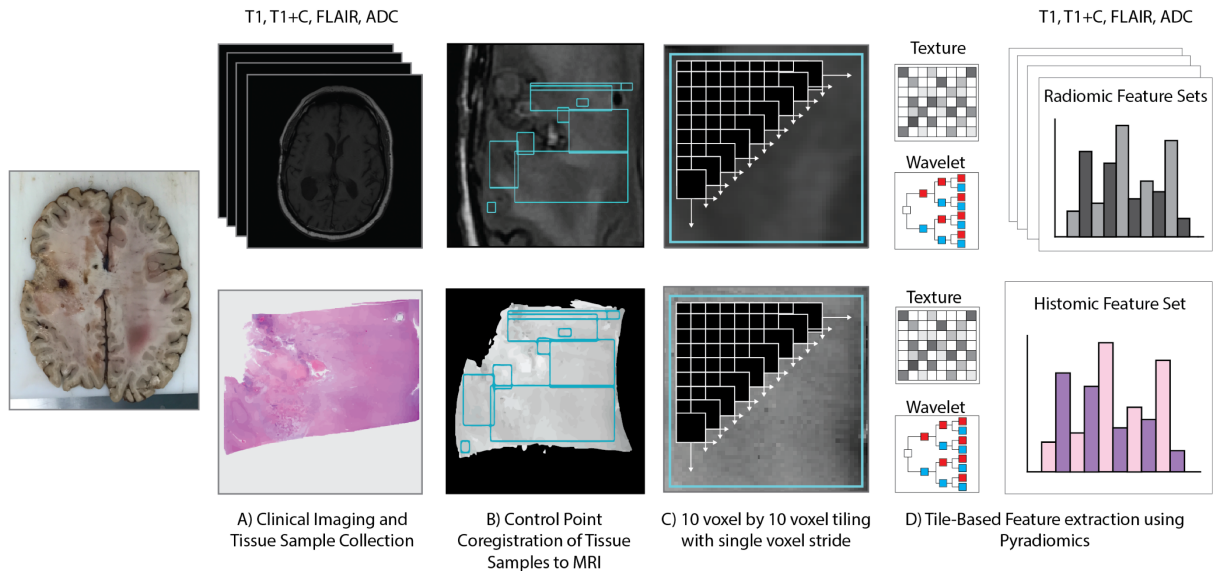


Figure 1: Schematic representation of the data collection process. For each subject, A) clinical MRI and HE-stained tissue samples of notable brain regions were collected, B) greyscale tissue samples were coregistered to the MRI using manual control point warping, C) tile masks were defined by using a 10 by 10 voxel frame with a single voxel stride across valid regions of the histology/MRI, and D) radiomic features were calculated across the tiles for each MR image and histomic features were calculated across the same tiles for the histology.

an example subject at 1.5T include (repetition time/echo time): T1 spin-echo sequence (T1), 666/14 ms; post contrast T1 spin-echo acquired with intravenous gadolinium (T1+C), 666/14 ms; apparent diffusion coefficient (ADC), calculated from diffusion-weighted images (DWI) acquired with an inversion recovery sequence using $B=0$ sec/mm² and $b=1000$ sec/mm², 10,000/90.7 ms; and FLAIR, acquired with an inversion recovery sequence, 10,000/151.8 ms and TI of 2,200 ms, all images acquired with submillimeter in-plane resolution.

All MR images for a given patient were rigidly aligned with the FLAIR image using FSLs FLIRT tool (2830). After co-registration, T1, T1+C, and FLAIR images were intensity normalized by dividing voxel intensity by its standard deviation across the whole brain (31). Images were visually inspected before and after processing to ensure images were free of any artifacts that may confound analyses.

2.3. *Ex-vivo Histology Processing*

Upon death, the brains of each subject were removed during autopsy and placed into 10 percent buffered formalin within a 3D-printed cage based on the subjects most recent MRI to maintain structural integrity with respect to the imaging data during fixation, as previously published (32). After approximately 2 weeks, the brain samples were sliced using slicing molds printed to delineate the axial slices from the most recent MRI. Tissue samples were collected from each subject based on enhancement on imaging, suspected presence of tumor, or pathologist-determined diagnostic relevance. The samples were then processed, embedded in paraffin, cut, and stained with hematoxylin and eosin (HE). The full slides were

photographed at 40X magnification using an Olympus sliding stage microscope. Matlab 2018b (MathWorks Inc. Natick, MA) was then used to process each individual tile, followed by down-sampling and compiling of all other tiles from the sample to generate a single image for each slide. Upon examination of these images, samples from each subject showed representative regions of both tumor and non-tumor characteristics, allowing assessment of the radiomic-histomic relationship across a range of tissue pathologies.

2.4. MRI-Histology Co-Registration

Previously published in-house software (Hist2MRI Toolbox, written in Matlab) was used to precisely align histology images to the MRI (19,3235). Manually defined control points were applied to align each composite histology image with the analogous anatomical features in the FLAIR sequence MRI. Digital photographs were taken at the time of the brain cutting and sample collection in order to precisely define the location of the histological sample with respect to the MRI. Samples were spatially aligned to the MRI slice that best represented the samples location by visually inspecting photographs of the brain slices acquired before and after each sample was collected (19,3235).

2.5. Feature Extraction

For each grayscale, MR-space histology image, regions of interest (ROI) were manually drawn to designate areas of the image with valid histological information (i.e. free from tears, folds). These ROIs were then used to generate tiles for use in radiomic feature extraction using a 10 voxel by 10 voxel sliding frame. Single-voxel strides in each dimension were used to define tiles across the ROIs (n=54,067), which were used as localized masks for calculation of the radiomic and histomic feature sets.

Pyradiomics v2.1.1 was used generate the radiomic and histomic feature sets for each tile (16,18). First order features (FO, n=18), gray level co-occurrence matrix (GLCM, n=24), gray level dependence matrix (GLDM, n=14), gray level run length matrix (GLRLM, n=16), gray level size zone matrix (GLSZM, n=16), and neighboring gray tone difference matrix (NGTDM, n=5) features were calculated for each MR image. The same features were additionally calculated on eight 3D wavelet decomposition (3DWD) images of each MRI, generated by applying all combinations of high and low pass filters in each dimension. This resulted in a total of 837 radiomic features per MRI modality. The same 837 features were then calculated for the grayscale histology image at MR-resolution for each tile, resulting in an analogous histomic feature set.

2.6. Statistical Analyses

2.6.1. Experiment 1: Correlative Analyses

In order to examine direct monotonic associations between analogous radiomic-histomic feature pairs, Spearman's rank correlations were computed between the radiomic feature from each MRI and its histomic analog. Peripheral analyses revealed that time between MR acquisition and death influenced the radiomic-histomic relationship (Supplemental Figure 1); thus, results are reported both before and after correction for this effect using partial Spearman correlations. Due to the large sample size of this analyses relative to the overall subject count, p-values were not considered a valuable indicator of meaningful effects; thus, effect sizes are reported here.

2.6.2. Experiment 2: Stability Analyses

Stability analyses were conducted in order to observe the effects of various confounding on the generalizability of radiomic-histomic relationships. The tile-wise log-Euclidean-distance (TLED) between the overall radiomic feature set of each MRI and the overall histomic feature set was used to assess global differences in radiomic-histomic associativity. The TLED probability density function for GE and Siemens scans collected at 3T were plotted to assess global effects of vendor, and the probability density function for 1.5T and 3T GE scans were plotted to assess global effects of field strength. Differences in distributions were quantified using the Kolmogorov-Smirnoff test.

In addition, feature-wise assessments of vendor and field strength effects were performed using linear mixed effect models. Separate models were fit to assess these effects on the normalized difference between each analogous radiomic-histomic pair. Two models were fit for each pair: 1) an assessment of vendor (GE vs. Siemens) as a main effect amongst subjects with MRI acquired at 3T and 2) an assessment of field strength (1.5T vs. 3T) as a main effect amongst subjects with MRI acquired using a GE scanner. Both models for each feature pair included time between MRI and death as a covariate, as well as random effects for subject and tissue sample.

3. Results

3.1. Experiment 1: Correlative Analyses

Figure 2 shows the resulting correlation heatmaps, displaying the Spearman's Rho between the radiomic and histomic version of each feature. FO features tended to show the strongest radiomic-histomic association, with very few GLCM, GLDM, GLRLM, GLSZM, and NGTDM features demonstrating meaningful radiomic-histomic relationships. Across the 3DWD images, the strength of association between FO features tended to increase, whereas higher order associations tended to dissipate across the wavelet decomposition images. Radiomic-histomic associations sorted by strength are presented in Figure 3 in order to compare feature strengths across image types, with T1+C and FLAIR images showing the strongest radiomic-histomic relationships. Overall, controlling for time between MR acquisition and death tended to decrease the strength of radiomic-histomic associations, but did not affect the general trends regarding image types and feature sets seen in the uncorrected data.

3.2. Experiment 2: Stability Analyses

TLED distributions for each confound analyses are presented in Figure 4. MR scanner vendor tended to have a larger influence on the overall TLED than field strength, though most scans displayed minor to moderate influence of both confounds on the overall TLED. The feature-wise assessment of these confounds is presented in Figure 5, which plots the standardized mixed model coefficient of the confounds against the radiomic-histomic association for each feature. These results confirm that differences in scanner vendor tend to outweigh differences in acquisition field strength. These plots also indicate that the features showing the strongest radiomic-histomic relationships tend to have less substantial confounding effects across most image modalities.

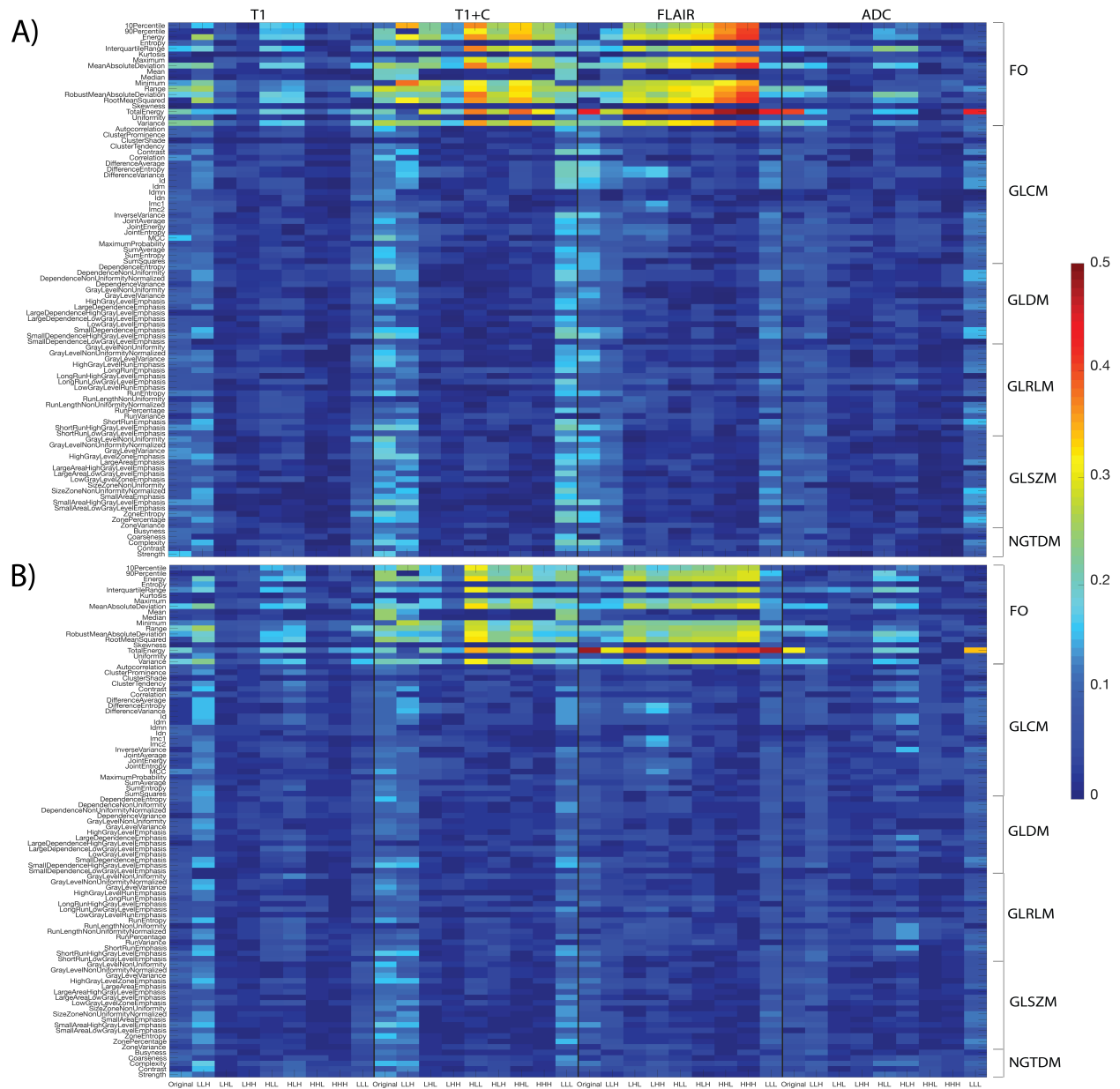


Figure 2: Heatmap of Spearman's Rho values between analogous radiomic-histomic feature pairs, presented by feature A) before and B) after correction for time between MRI and death. Note, first order features in general showed greater radiomic-histomic associations than the other five categorical feature sets.

4. Discussion

This study explored the histological underpinnings of tile-based MP-MRI radiomic features in GBM and other brain cancer patients. Several radiomic features demonstrated substantial associations with their histomic analogs, suggesting that these aspects of the MRI directly characterize the same features of the underlying tissue histology. These features are shown to be relatively robust across different confounding factors, such as MR scanner vendor and acquisition field strength. These findings, taken as a whole, begin to provide a neuroanatomical context for radiomics-based models of brain cancer characteristics.

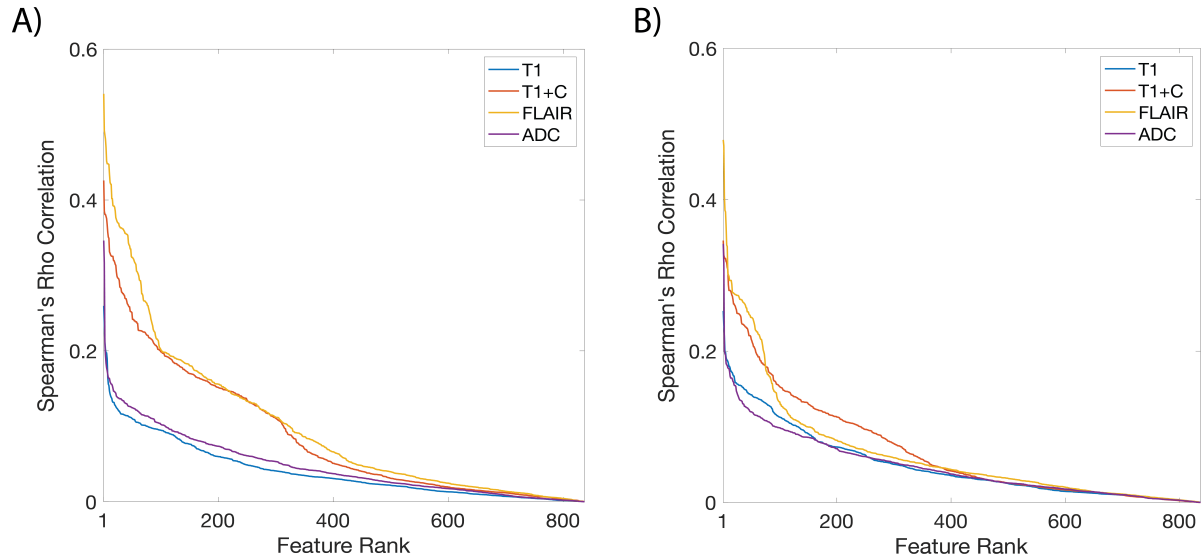


Figure 3: Ranked feature associations for each MR image contrast A) before and B) after correction for time between MRI and death. The FLAIR image generally shows the strongest associations, closely followed by the T1+C image.

To the best of our knowledge, this study is the first assessment of localized relationships between radiomic features and analogous histomic features calculated on histology samples. Our findings suggest that radiomic features are able to capture localized information about the underlying histology of the tissue, motivating a thrust towards radiomics-based models for localized tissue information. Past studies attempting to map localized tissue information using MRI have focused on the use of biopsy cores as the source of ground truth (3740). While this allows for characterization of tumor in the MRI-enhancing region, the use of autopsy samples in this study enabled an assessment of the radiomic-histomic relationship in both tumor and non-tumor tissue. Whole brain generalizability will improve the clinical utility of MRI-based tissue feature maps. Thus, this study motivates future investigations using autopsy samples as ground truth in order to capture whole-brain heterogeneity of tissue features.

Despite the benefits of measuring the radiomic-histomic relationship across autopsy samples, the time between the MRI scan and tissue fixation at death becomes a new confounding factor, as subtle changes in the disease state may occur during this time. When assessing radiomic-histomic relationships after controlling for the duration of this period, nearly all features show mild to moderate decreases in associative strength. Despite these effects, the overall strength and patterns of association remained largely intact, suggesting that minor statistical artifacts in the uncorrected data did not falsely manifest these general trends. Larger studies are thus warranted to better assess the validity of this claim, as well as to provide better characterizations of MRI-to-fixation duration effects on different MRI-to-tissue mappings.

The most notable contrasts within the associative analyses (Figure 2) include the general strength of FO features compared to various higher order features, as well as the modulation of this relationship across the 3DWT. Generally, FO features presented with more substantial

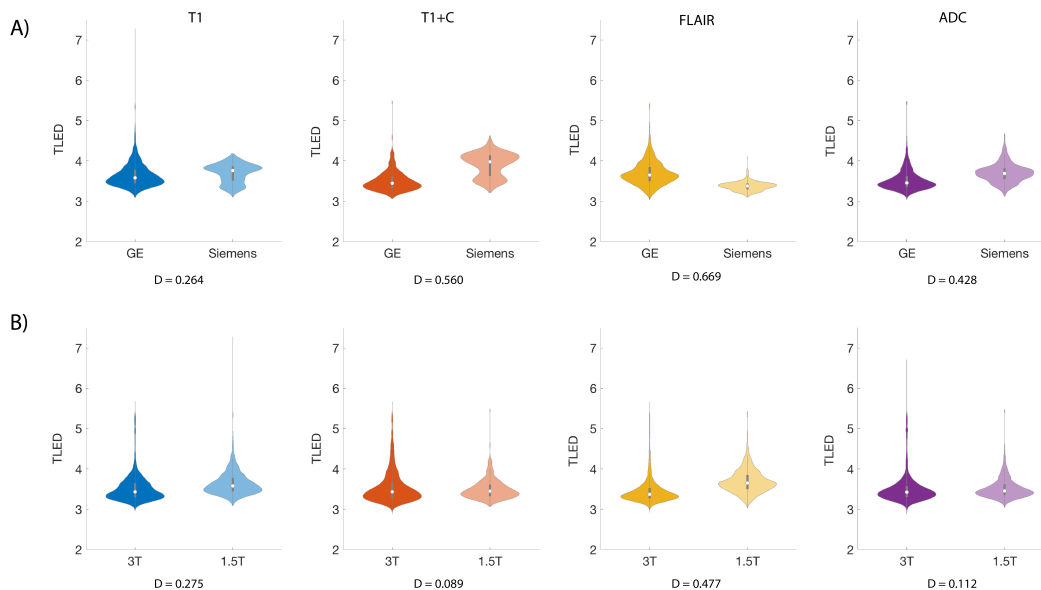


Figure 4: Distributions of Tile-wise Log Euclidean Distance (TLED) between radiomic and histomic features, grouped by A) scanner vendor, and B) acquisition field strength. Differences in distributions, quantified by K-S statistic D , indicate different radiomic-histomic similarity distributions between classes. Both factors show modest to substantial influences on the overall radiomic-histomic relationship, though these results suggest scanner vendor may be a stronger overall confound than acquisition field strength.

associations than those of higher order features, though higher order features of the T1+C and FLAIR images still showed some weak associations. This split in associative strength was compounded by the 3DWT results, with FO features increasing in associative strength and higher order features decreasing in strength across most wavelet decompositions. The lower frequency wavelet decompositions (LLL and LLH) deviated from this pattern and showed some increase in higher-order associations. Future research into the inter-feature relationships will provide insight as to whether or not these wavelet decompositions provide new information or simply preserve higher order associations found in the original image.

Comparing across scan types, the FLAIR image tended to have the strongest associations with histology texture (Figure 3). Given the immense diagnostic utility of FLAIR images in delineating different tumor regions, this does not come as a great surprise, and supports our use of the FLAIR image as the optimal reference image for histology co-registration. The T1+C image also demonstrated substantial radiomic-histomic associations, which suggests that the addition of contrast agent enhances the degree of texture preservation seen in the MRI. The features of the T1+C image with the strongest radiomic-histomic relationships also tended to be more stable across scanner vendor and acquisition field strength than those of the FLAIR. These results suggest that the contrast agent may provide new information relevant to tissue texture beyond that of the standard T1 image, which showed substantially weaker radiomic-histomic associations.

The weak radiomic-histomic associations observed in the T1 and ADC image relative to the FLAIR and T1+C images imply that these MRI modalities are not as representative

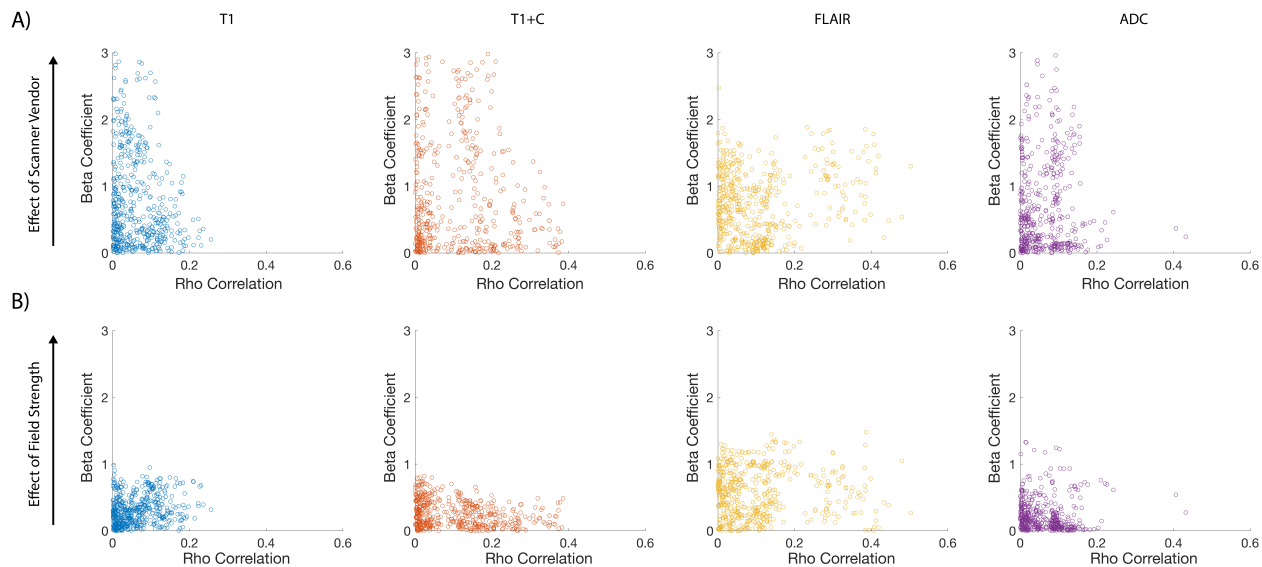


Figure 5: Effects of A) scanner vendor and B) acquisition field strength presented by feature. Each plot shows the standardized beta coefficient from each mixed model analyses, plotted against the radiomic-histomic association for each feature. Aside from the FLAIR image, features with the highest radiomic-histomic associations tended to show the lowest influences of scanner vendor and acquisition field strength.

of underlying tissue histology texture. This does not necessarily discount the predictive utility of these images as much as it highlights what sort of information these modalities may provide. Whereas the magnitude of the ADC image in a given region may provide robust and insightful information regarding some diagnostic criteria, the features of the ADC and T1 images may not be as relevant to providing histological texture information. This distinction is important as studies move towards assessing the biological underpinnings of radiomics. The lack of texture preservation seen in these results point future studies towards non-textural candidates for biological validation of radiomic features derived from these modalities.

A clinical degree of MR scanner and field strength heterogeneity was present in the MR acquisitions of this sample, which was used to examine the influence of these factors on the radiomic-histomic relationship. Previous studies have demonstrated several radiomic features susceptible to differences across different scanners (4143); this study adds to this literature by providing a breakdown of how well features represent histological texture across scanner vendor and field strength. As desired, the features with the greatest degree of association between radiomic and histomic analogs tended to have the least substantial effects of scanner and field strength, with the notable exception of the evenly-confounded FLAIR features. Statistical artifacts of the confounds may influence the weaker associations observed in this data set, but generally these results point to a subset of features characterized by both strong and stable radiomic-histomic associations. Larger follow-up studies assessing radiomic-histomic relationships may be able to reveal additional features that accurately characterize tissue texture for particular scanner vendors and acquisition parameters.

This study is not without its limitations, however. The relatively small sample size of this study calls for replication of these results in larger data sets to confirm the generalizability of the patterns seen here. This study was also limited to primary brain cancer patients, which

limits the scope of the radiomic-histomic relationship these results imply. Future studies of radiomic-histomic relationships in other diseases will be an important step in establishing more general cases for the relationship between MRI and tissue texture. The use of a tile-based prediction to study localized information does not allow for the use of shape- and size-based radiomic features, which often provide useful weights in radiomics-based modeling of prognostic factors. Though this study statistically controlled for the duration between MRI acquisition and death, it is possible that these effects are not adequately addressed as covariates in this small sample. Future, large-scale studies of autopsy data will be essential to characterize the magnitude of this effect, as well as to address optimal strategies to account for these effects.

In conclusion, this study provides a novel characterization of the radiomic-histomic relationship in an attempt to provide a neuroanatomical basis for radiomics analyses. These results show a substantial degree of heterogeneity in the strength and stability of radiomic-histomic relationships but reveal a subset of radiomic features that stably reflect information about the underlying histology. This study provides the groundwork for future investigations into the quantitative pathological validation of radiomics analyses as currently performed, as well as underscores an opportunity for radiomics-based predictions of localized histological features with diagnostic and prognostic utility.

5. Acknowledgements

We would like to thank our patients for their participation in this study and our funding sources: American Brain Tumor Association DG14004, R01CA218144, R01CA218144-02S1, and R21CA23189201.

6. Disclosures

The authors of this manuscript have no disclosures to report.

References

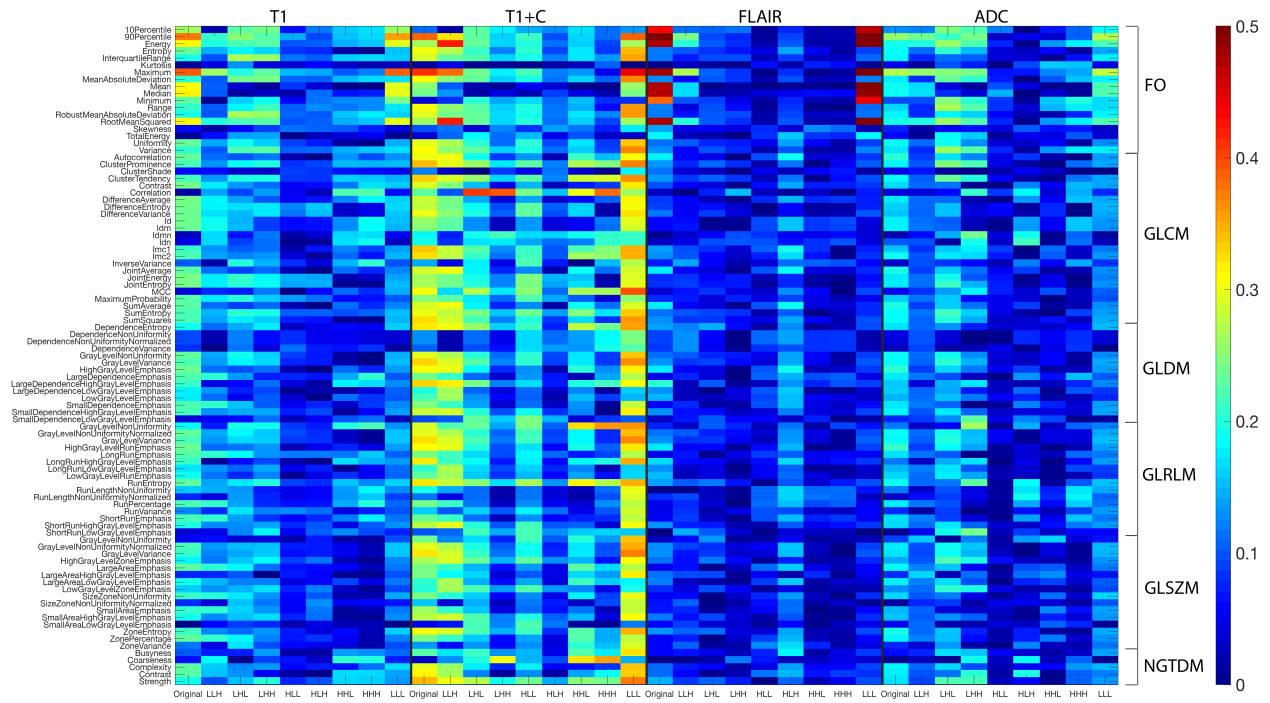
- [1] Ostrom QT, Bauchet L, Davis FG, Deltour I, Fisher JL, Langer CE, et al. The epidemiology of glioma in adults: a state of the science review. *Neuro Oncol.* 2014 Jul;16(7):896913.
- [2] Batash R, Asna N, Schaffer P, Francis N, Schaffer M. Glioblastoma Multiforme, Diagnosis and Treatment; Recent Literature Review. *Curr Med Chem.* 2017;24(27):30029.
- [3] Margiewicz S, Cordova C, Chi AS, Jain R. State of the Art Treatment and Surveillance Imaging of Glioblastomas. *Semin Roentgenol.* 2018 Jan;53(1):2336.
- [4] Shukla G, Alexander GS, Bakas S, Nikam R, Talekar K, Palmer JD, et al. Advanced magnetic resonance imaging in glioblastoma: a review. *Chinese Clin Oncol.* 2017 Aug;6(4):40.

- [5] Toh CH, Castillo M. Early-Stage Glioblastomas: MR Imaging-Based Classification and Imaging Evidence of Progressive Growth. *AJNR Am J Neuroradiol*. 2017 Feb;38(2):28893.
- [6] Durand-Munoz C, Flores-Alvarez E, Moreno-Jimenez S, Roldan-Valadez E. Pre-operative apparent diffusion coefficient values and tumour region volumes as prognostic biomarkers in glioblastoma: correlation and progression-free survival analyses. *Insights Imaging*. 2019 Mar;10(1):36.
- [7] Galla N, Chiang G, Chakraborty S, Singh R, John Tsiouris A, Boockvar J, et al. Apparent diffusion coefficient changes predict survival after intra-arterial bevacizumab treatment in recurrent glioblastoma. *Neuroradiology*. 2017 May;59(5):499505.
- [8] Yoon RG, Kim HS, Kim DY, Hong GS, Kim SJ. Apparent diffusion coefficient parametric response mapping MRI for follow-up of glioblastoma. *Eur Radiol*. 2016 Apr;26(4):103747.
- [9] Suo S, Cao M, Zhu W, Li L, Li J, Shen F, et al. Stroke assessment with intravoxel incoherent motion diffusion-weighted MRI. *NMR Biomed*. 2016 Mar;29(3):3208.
- [10] Artzi M, Aizenstein O, Jonas-Kimchi T, Myers V, Halleivi H, Ben Bashat D. FLAIR lesion segmentation: application in patients with brain tumors and acute ischemic stroke. *Eur J Radiol*. 2013 Sep;82(9):15128.
- [11] Lestro Henriques I, Gutierrez-Fernandez M, Rodriguez-Frutos B, Ramos-Cejudo J, Otero-Ortega L, Navarro Hernanz T, et al. Intralesional Patterns of MRI ADC Maps Predict Outcome in Experimental Stroke. *Cerebrovasc Dis*. 2015;39(56):293301.
- [12] Kumar V, Gu Y, Basu S, Berglund A, Eschrich SA, Schabath MB, et al. Radiomics: the process and the challenges. *Magn Reson Imaging [Internet]*. 2012/08/13. 2012 Nov;30(9):123448.
- [13] Park JE, Kim HS. Radiomics as a Quantitative Imaging Biomarker: Practical Considerations and the Current Standpoint in Neuro-oncologic Studies. *Nucl Med Mol Imaging (2010) [Internet]*. 2018/02/01. 2018 Apr;52 (2):99108.
- [14] Lambin P, Rios-Velazquez E, Leijenaar R, Carvalho S, van Stiphout RGPM, Granton P, et al. Radiomics: extracting more information from medical images using advanced feature analysis. *Eur J Cancer [Internet]*. 2012/01/16. 2012 Mar;48(4):4416.
- [15] Gillies RJ, Kinahan PE, Hricak H. Radiomics: Images Are More than Pictures, They Are Data. *Radiology [Internet]*. 2015/11/18. 2016 Feb;278(2):56377.
- [16] van Griethuysen JJM, Fedorov A, Parmar C, Hosny A, Aucoin N, Narayan V, et al. Computational Radiomics System to Decode the Radiographic Phenotype. *Cancer Res [Internet]*. 2017 Nov 1;77(21):e104 LP-e107.
- [17] Wang Y, Che X, Ma S. Nonlinear filtering based on 3D wavelet transform for MRI denoising. *EURASIP J Adv Signal Process [Internet]*. 2012;2012(1):40.

- [18] Lee G, Gommers R, Waselewski F, Wohlfahrt K, O’Leary A. PyWavelets: A Python package for wavelet analysis. *J Open Source Softw* [Internet]. 2019 Apr 12;4(36):1237.
- [19] McGarry SD, Hurrell SL, Kaczmarowski AL, Cochran EJ, Connelly J, Rand SD, et al. Magnetic Resonance Imaging-Based Radiomic Profiles Predict Patient Prognosis in Newly Diagnosed Glioblastoma Before Therapy. *Tomogr (Ann Arbor, Mich)*. 2016 Sep;2(3):2238.
- [20] Lu C-F, Hsu F-T, Hsieh KL-C, Kao Y-CJ, Cheng S-J, Hsu JB-K, et al. Machine LearningBased Radiomics for Molecular Subtyping of Gliomas. *Clin Cancer Res*. 2018;24(18):442936.
- [21] Li Z-C, Bai H, Sun Q, Zhao Y, Lv Y, Zhou J, et al. Multiregional radiomics profiling from multiparametric MRI: Identifying an imaging predictor of IDH1 mutation status in glioblastoma. *Cancer Med*. 2018 Dec;7(12):59996009.
- [22] Kickingereder P, Gotz M, Muschelli J, Wick A, Neuberger U, Shinohara RT, et al. Large-scale Radiomic Profiling of Recurrent Glioblastoma Identifies an Imaging Predictor for Stratifying Anti-Angiogenic Treatment Response. *Clin Cancer Res*. 2016 Dec;22(23):576571.
- [23] Sanghani P, Ang BT, King NKK, Ren H. Overall survival prediction in glioblastoma multiforme patients from volumetric, shape and texture features using machine learning. *Surg Oncol*. 2018 Dec;27(4):70914.
- [24] Li Q, Bai H, Chen Y, Sun Q, Liu L, Zhou S, et al. A Fully-Automatic Multiparametric Radiomics Model: Towards Reproducible and Prognostic Imaging Signature for Prediction of Overall Survival in Glioblastoma Multiforme. *Sci Rep*. 2017 Oct;7(1):14331.
- [25] He L, Huang Y, Ma Z, Liang C, Liang C, Liu Z. Effects of contrast-enhancement, reconstruction slice thickness and convolution kernel on the diagnostic performance of radiomics signature in solitary pulmonary nodule. *Sci Rep*. 2016 Oct;6:34921.
- [26] Kickingereder P, Neuberger U, Bonekamp D, Piechotta PL, Gotz M, Wick A, et al. Radiomic subtyping improves disease stratification beyond key molecular, clinical, and standard imaging characteristics in patients with glioblastoma. *Neuro Oncol*. 2018 May;20(6):84857.
- [27] Park JE, Park SY, Kim HJ, Kim HS. Reproducibility and Generalizability in Radiomics Modeling: Possible Strategies in Radiologic and Statistical Perspectives. *Korean J Radiol* [Internet]. 2019 Jul;20(7):112437.
- [28] Jenkinson M, Bannister P, Brady M, Smith S. Improved optimization for the robust and accurate linear registration and motion correction of brain images. *Neuroimage*. 2002 Oct;17(2):82541.
- [29] Jenkinson M, Smith S. A global optimisation method for robust affine registration of brain images. *Med Image Anal*. 2001 Jun;5(2):14356.

- [30] Jenkinson M, Beckmann CF, Behrens TEJ, Woolrich MW, Smith SM. FSL. *Neuroimage*. 2012 Aug;62(2):78290.
- [31] Ellingson BM, Kim HJ, Woodworth DC, Pope WB, Cloughesy JN, Harris RJ, et al. Recurrent glioblastoma treated with bevacizumab: contrast-enhanced T1-weighted subtraction maps improve tumor delineation and aid prediction of survival in a multicenter clinical trial. *Radiology*. 2014 Apr;271 (1):20010.
- [32] Nguyen HS, Milbach N, Hurrell SL, Cochran E, Connelly J, Bovi JA, et al. Progressing Bevacizumab-Induced Diffusion Restriction Is Associated with Coagulative Necrosis Surrounded by Viable Tumor and Decreased Overall Survival in Patients with Recurrent Glioblastoma. *AJNR Am J Neuroradiol*. 2016 Dec;37(12):22018.
- [33] Bukowy JD, Foss H, McGarry SD, Lowman A, Hurrell S, Ickzkowski KA, et al. Accurate segmentation of prostate cancer histomorphometric features using a weakly supervised convolutional neural network. *FASEB J [Internet]*. 2019;33(1):lb12.
- [34] McGarry SD, Hurrell SL, Iczkowski KA, Hall W, Kaczmarowski AL, Banerjee A, et al. Radio-pathomic Maps of Epithelium and Lumen Density Predict the Location of High-Grade Prostate Cancer. *Int J Radiat Oncol Biol Phys*. 2018 Aug;101(5):117987.
- [35] McGarry SD, Bukowy JD, Iczkowski KA, Unteriner JG, Duvnjak P, Lowman AK, et al. Gleason Probability Maps: A Radiomics Tool for Mapping Prostate Cancer Likelihood in MRI Space. *Tomogr (Ann Arbor, Mich)*. 2019 Mar;5(1):12734.
- [36] Zwanenburg A, Leger S, Vallieres M, Lck S, Initiative for. Image biomarker standardisation initiative - feature definitions. 2016 Dec 21;
- [37] Gates EDH, Lin JS, Weinberg JS, Hamilton J, Prabhu SS, Hazle JD, et al. Guiding the first biopsy in glioma patients using estimated Ki-67 maps derived from MRI: conventional versus advanced imaging. *Neuro Oncol*. 2019 Mar;21(4):52736.
- [38] Hu LS, Ning S, Eschbacher JM, Baxter LC, Gaw N, Ranjbar S, et al. Radiogenomics to characterize regional genetic heterogeneity in glioblastoma. *Neuro Oncol*. 2017 Jan;19(1):12837.
- [39] Prah MA, Al-Gizawiy MM, Mueller WM, Cochran EJ, Hoffmann RG, Connelly JM, et al. Spatial discrimination of glioblastoma and treatment effect with histologically-validated perfusion and diffusion magnetic resonance imaging metrics. *J Neurooncol*. 2018 Jan;136(1):1321.
- [40] Chang PD, Malone HR, Bowden SG, Chow DS, Gill BJA, Ung TH, et al. A Multiparametric Model for Mapping Cellularity in Glioblastoma Using Radiographically Localized Biopsies. *AJNR Am J Neuroradiol*. 2017 May;38(5):8908.
- [41] Chirra P, Leo P, Yim M, Bloch BN, Rastinehad AR, Purysko A, et al. Multisite evaluation of radiomic feature reproducibility and discriminability for identifying peripheral zone prostate tumors on MRI. *J Med imaging (Bellingham, Wash)*. 2019 Apr;6(2):24502.

- [42] Saha A, Yu X, Sahoo D, Mazurowski MA. Effects of MRI scanner parameters on breast cancer radiomics. *Expert Syst Appl.* 2017 Nov;87:38491.
- [43] Um H, Tixier F, Bermudez D, Deasy JO, Young RJ, Veeraraghavan H. Impact of image preprocessing on the scanner dependence of multi-parametric MRI radiomic features and covariate shift in multi-institutional glioblastoma datasets. *Phys Med Biol.* 2019 Aug;64(16):165011.



Supplemental Figure 1: Spearman's Rho associations between the normalized radiomic-histomic feature difference and time between MRI and death, presented by feature.